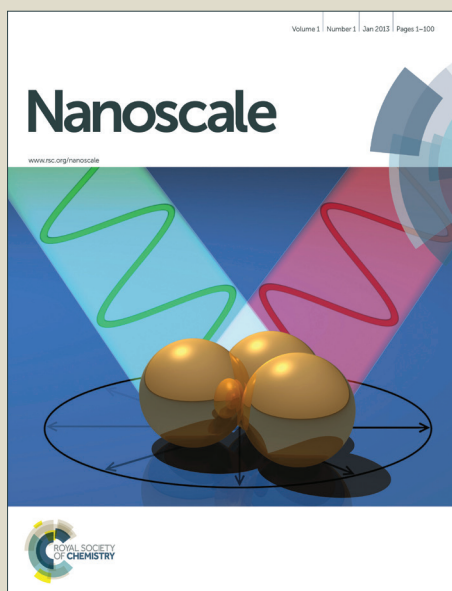


Nanoscale

Accepted Manuscript



This is an *Accepted Manuscript*, which has been through the Royal Society of Chemistry peer review process and has been accepted for publication.

Accepted Manuscripts are published online shortly after acceptance, before technical editing, formatting and proof reading. Using this free service, authors can make their results available to the community, in citable form, before we publish the edited article. We will replace this *Accepted Manuscript* with the edited and formatted *Advance Article* as soon as it is available.

You can find more information about *Accepted Manuscripts* in the [Information for Authors](#).

Please note that technical editing may introduce minor changes to the text and/or graphics, which may alter content. The journal's standard [Terms & Conditions](#) and the [Ethical guidelines](#) still apply. In no event shall the Royal Society of Chemistry be held responsible for any errors or omissions in this *Accepted Manuscript* or any consequences arising from the use of any information it contains.

Edge Reconstruction-Mediated Graphene Fracture

Ziang Zhang[†], Alex Kutana[†], and Boris I. Yakobson^{†*}

[†]*Department of Materials Science and Nanoengineering, Rice University, Houston, TX 77005*

Abstract

Creation of free edges in graphene during mechanical fracture is a process that is important from both fundamental and technological points of view. Here we derive an analytical expression for the energy of a free-standing reconstructed chiral graphene edge, with chiral angle varying from 0° to 30° , and test it by first principle computations. We then study the thermodynamics and kinetics of fracture and show that during graphene fracture under uniaxial load it is possible obtain fully reconstructed zigzag edges through sequential reconstructions at the crack tip. The preferable condition for this process is high temperature ($T \sim 1000$ K) and low (quasi-static) mechanical load ($K_I \sim 5.0$ eV/Å^{5/2}). Edge configurations of graphene nanoribbons may be tuned according to these guidelines.

Keywords

Graphene, fracture, edge reconstruction, edge chirality, Griffith theory, lattice trapping effect, metastable states, first-principles calculations.

Since the discovery of its physics by Geim and Novoselov in 2007,¹ graphene, a two-dimensional carbon nanomaterial, has been the focus of nanoscience research for its outstanding mechanical,² electronic,³ and chemical properties.⁴ Graphene has many

attractive potential applications, including transistors,⁵ energy storage,⁶ solar cells,⁷ and spintronics.⁸

Many graphene-based prototype devices are realized using graphene nanoribbons (GNRs)⁹⁻¹¹ - sheets of graphene with widths of several angstroms and varying edge chiralities. The edges of graphene nanoribbons strongly affect their mechanical¹² and electronic^{11, 13} properties. Therefore, the study of graphene edges is important to the understanding of graphene nanoribbons.

Graphene edges consisting of only hexagonal cells are referred to as pristine edges, and are classified by their chiral angles. Among all types of pristine edges, “armchair” (AC) edges (with a chiral angle of 30°) and “zigzag” (ZZ) edges (with a chiral angle of 0°) are geometrically most simple, and may be considered as the basic geometrical components of other edges.¹⁴ AC edges have fully saturated chemical bonds and are thus chemically passive and energetically stable, with formation energies ~ 1.00 eV/Å.¹⁴ ZZ edges, on the other hand, have unpaired electrons, leading to higher chemical reactivity and higher formation energy (~ 1.21 eV/Å).¹⁴ Electronic properties of ZZ edges range from metallic to semiconducting, depending on the nanoribbon width, and AC edges are always semiconducting.¹³ As edges with chiral angles between 0° (AC) and 30° (ZZ) are obtained from AC and ZZ segments, they are believed to have energies also between that of AC and ZZ edges. This assumption is supported by computation results.¹⁴

Traditionally, pristine edges were believed to be the only possible configurations for graphene edges. It was not until 2008 that Koskinen *et al.*¹⁵ made a theoretical prediction of reconstructed edges – a new, more stable configuration that consists of alternating pentagon-heptagon pairs. The name “reconstructed edges” indicates that they can be

obtained by reconstruction – a process in which two adjacent hexagons reconstruct into one pentagon-heptagon pair. Reconstructed ZZ edges (ZZ57) have paired atoms similar to those of armchair edges, and are chemically passive and energetically favorable (~ 0.98 eV/Å). Besides being more stable, ZZ57 edges are semiconducting rather than metallic. It should be mentioned here that two possible types of reconstructed AC edges were also explored, but these edges are much less energetically favorable than pristine AC edges.¹⁵ Therefore in this paper the name “reconstructed edges” stands only for ZZ57, unless specifically noted.

As edge reconstruction has important impact on the electronic and chemical properties of GNRs and other graphene-based materials, numerous follow-up studies were undertaken. Koskinen *et al.* (2009),¹⁶ Girit *et al.* (2009),¹⁷ and Kim *et al.* (2013)¹⁸ observed the occurrence of graphene edge reconstruction in experiment. Theoretical studies focusing on the properties of reconstructed edges have also been done, some investigating its electronic properties,^{19,20} while others considering factors such as mechanical strain²¹ and accommodation of non-carbon atoms.^{22,23}

Besides the properties of already reconstructed graphene edges, it is also of great interest and importance to study the process of reconstruction and the conditions that allow the process to occur. Kinetic studies on the activation barrier from pristine edge to reconstructed edge have been conducted by various researchers. In their same paper that proposed the configuration of the reconstructed edge, Koskinen *et al.*¹⁵ mentioned briefly that the energy barrier for reconstruction obtained by DFT calculation is ~ 0.6 eV/Å. Kroes *et al.*²⁴ applied an umbrella-sampling MC method, and found that the reaction energy barrier of the first reconstruction on a pristine zigzag edge is 0.83 eV/Å, while the

barriers for subsequent reconstruction processes gradually become lower, until reaching 0.6 eV/Å, due to the influence of pre-formed pentagon-heptagon pairs. The moderate reaction barrier of reconstruction on free-standing edges indicates that edge reconstruction may well take place under thermal fluctuation or mechanical processes such as tension or fracture.

Because graphene sheets and nanoribbons are usually synthesized by mechanical exfoliation,²⁵ it is important to get insight into the feasibility of edge reconstruction during mechanical fracture, and if such a process be possible, its mechanism and energetics. Although there are many works²⁶⁻²⁹ on the fracture process of graphene sheets (for instance, Kim *et al.*²⁶ conducted a molecular dynamics simulation showing that armchair and zigzag chirality angles are the ones that are most frequently obtained by graphene ripping), there are fewer works that couple the process of reconstruction with fracture. Terdalkar *et al.*³⁰ conducted MD simulations according to the Griffith theory of elastic fracture³¹ and proposed several schemes in which reconstruction occurs occasionally during ripping. Their work provides insight into how reconstruction may initiate during fracture. The question “if possible, under what condition can reconstruction occur continuously on pristine edges during fracture” remains crucial in the field of graphene mechanics, and is the focus of our study. Below we show that, during the fracture process of a monolayer graphene sheet, reconstruction is preferred over direct bond breaking, both thermodynamically and kinetically, leading to the formation of nanoribbons with completely reconstructed edges.

Results and Discussion

Energy of Reconstructed Edge from Armchair to Zigzag. For an edge of a certain chiral angle, there are technically infinite configuration possibilities, depending on the arrangement of AC and ZZ lattices along the edge. In our study we choose the configuration that follows the edge's chirality most closely, i.e. ones that run in straight line in which the AC and ZZ cells are most evenly distributed. This principle does not undermine the generality of our study, as all other configurations can be decomposed into a combination of edges with lower chirality indices.

With this principle established, we are now able to derive the energetics for graphene edges of any chirality. A segment of a graphene edge defined by a translation vector $\mathbf{T} = n\mathbf{a}_1 + m\mathbf{a}_2$ can be denoted in two ways: by its chiral angle χ , or by a pair of chiral indices (n, m) .¹⁴ The two notations are interchangeable. For a segment of graphene edge (n, m) , there are $n - m$ zigzag atoms and $2m$ armchair atoms. The ratio between lengths of zigzag and armchair segments is $(n - m)/\sqrt{3}m$, and we have:

$$\frac{n - m}{\sin(30 - \chi)} = \frac{\sqrt{3}m}{\sin \chi} \quad (1)$$

Therefore,

$$\chi = \tan^{-1} \frac{\sqrt{3}m}{2n + m} \quad (2)$$

The energy of a pristine graphene edge per unit length¹⁴ with chiral angle $0^\circ < \chi < 30^\circ$ is:

$$\epsilon_{pris}(\chi) = 2\epsilon_{ac} \sin \chi + 2\epsilon_{zz} \sin(30 - \chi) \quad (3)$$

Here, χ is chiral angle, $\epsilon_{ac} = 1.00 \text{ eV/\AA}$ is the energy per unit length for AC edge, and $\epsilon_{zz} = 1.21 \text{ eV/\AA}$ is the energy per unit length for ZZ edge.

The energy per unit length for reconstructed graphene edge can be described by a more complex piecewise function as:

$$\epsilon_{rec}(\chi) = \begin{cases} \epsilon_1(\chi), & 0 \leq u - k < \frac{1}{2}, k = [u] \\ \epsilon_2(\chi), & \frac{1}{2} \leq u - k < 1 \end{cases} \quad (4)$$

In eq 4,

$$\epsilon_1 = 2 \left[\epsilon_{AC} + \frac{2}{\sqrt{3}} k (\epsilon_{ZZ57} - \epsilon_{ZZ6}) \right] \sin \chi + 2\epsilon_{ZZ6} \sin(30 - \chi) + \delta(\chi) \quad (5)$$

$$\begin{aligned} \epsilon_2 = 2 \left[\epsilon_{AC} + \frac{2}{\sqrt{3}} (k + 1) (\epsilon_{ZZ6} - \epsilon_{ZZ57}) \right] \sin \chi \\ + 2(2\epsilon_{ZZ57} - \epsilon_{ZZ6}) \sin(30 - \chi) + \delta(\chi) \end{aligned} \quad (6)$$

$u = (n - m)/2m = \sqrt{3} \sin(30 - \chi) / 2 \sin \chi$ is the ratio of number of zigzag atoms over armchair atoms, and $k = [u]$ is the largest integer no greater than u .

In the special case of a reconstructed zigzag edge, an appropriate limit should be taken in eq 4, yielding, as expected, $\epsilon_1(\chi = 0) = \epsilon_2(\chi = 0) = \epsilon_{ZZ57}$.

In the equations above, $\epsilon_{zz57} = 0.98 \text{ eV/\AA}$ is the energy per unit length for ZZ57 edge, and $\delta(\chi)$ is the junction energy per unit length, which is given by:

$$\delta(\chi) = \begin{cases} 0, & 0 \leq u < \frac{1}{2} \\ \frac{2\Delta[\sqrt{3} \sin(30 - \chi) - \sin \chi]}{\sqrt{3}L}, & \frac{1}{2} \leq u < 1 \\ \frac{2\Delta \sin \chi}{\sqrt{3}L}, & u \geq 1 \end{cases} \quad (7)$$

In eq 7, $L = 2.459 \text{ \AA}$ is the graphene lattice parameter, and $\Delta = 0.96 \text{ eV}$, is the energy of one junction, i.e. the distortion energy resulting from the lattice distortion at the connection between a hexagon (AC lattice or ZZ lattice) and a pentagon-heptagon pair (ZZ57 lattice). From the DFT simulation we obtain $\Delta = 0.96 \text{ eV}$.

In order to validate our model, we ran a series of DFT simulations on graphene edges of various chiral angles. The comparison between our analytical derivation and simulation results shows good agreement between analytical formula eqs 4-6 and directly computed energies, as shown in Figure 1. From the results we can also see that, ZZ57 edges and AC edges are most energetically favorable among edges of all chiralities.

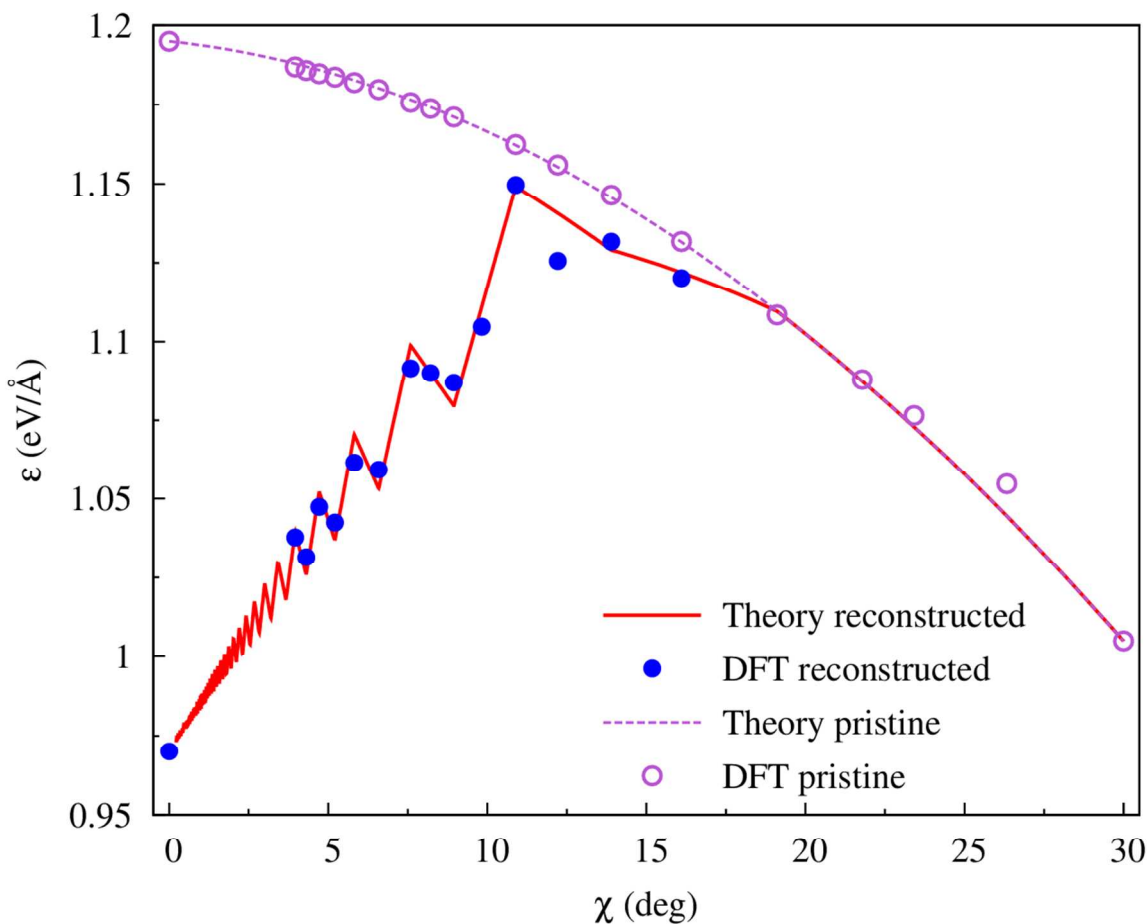


Figure 1. Energies per unit length of pristine and reconstructed edges: comparison between analytical formula eq 4 and DFT simulations. We can see that ZZ57 edges and AC edges are most energetically favorable among edges of all directions.

Reconstructed Edges are more Stable. Since mechanical exfoliation and concomitant fracture, or the fracture in nanotube unzipping, are among the most common methods to obtain graphene nanoribbons, it would be of great practical interest to study the mechanism of edge reconstruction during graphene fracture. According to the above analysis on the energetics of static edges, it is known that ZZ57 edges are the most favorable among all edges. In the remaining part of our work we will study the process in

which reconstructed pentagon-heptagon pairs form during graphene fracture, and determine the loading conditions that allow this process to occur.

How Do Crack Tips Reconstruct during Fracture? Figure 2 shows the process of the paired edge reconstruction at the crack tip of graphene fracture, using a set of snapshots obtained from our molecular dynamics simulation. Step 1 shows the original configuration where the two edges by the crack tip consist of pure hexagons. Atoms 5 and 6 (colored in blue) have a bond distance of 1.8 Å, suggesting strong bonding. Atoms 1 and 2 (colored in green), on the other hand, have a distance of 2.5 Å, suggesting little interaction. During the fracture process, atoms 3 and 4 are respectively pulled by atoms 5 and 6 along the bond directions, because atoms 5 and 6 are connected with a covalent bond and attract each other. Atoms 1 and 2, however, are not similarly pulled by strong forces. As a result of different forces received by its two atoms, the bond linking atoms 1 and 3 would rotate clockwise. Similarly, the bond between atoms 2 and 4 would rotate counter-clockwise. The paired bond rotations facilitated by the attraction between the two atoms near crack tip, as depicted in Steps 2 to 3 eventually results in edge reconstruction during fracture and the formation of two pentagon-heptagon pairs, as shown in Step 6.

After establishing the mechanism to obtain pentagon-heptagon pairs – and eventually, ZZ 57 edges – by means of graphene fracture, we proceed to explore its validity by mechanical and energetic analysis. We start by introducing a crack tip model for simulating quasistatic graphene fracture.

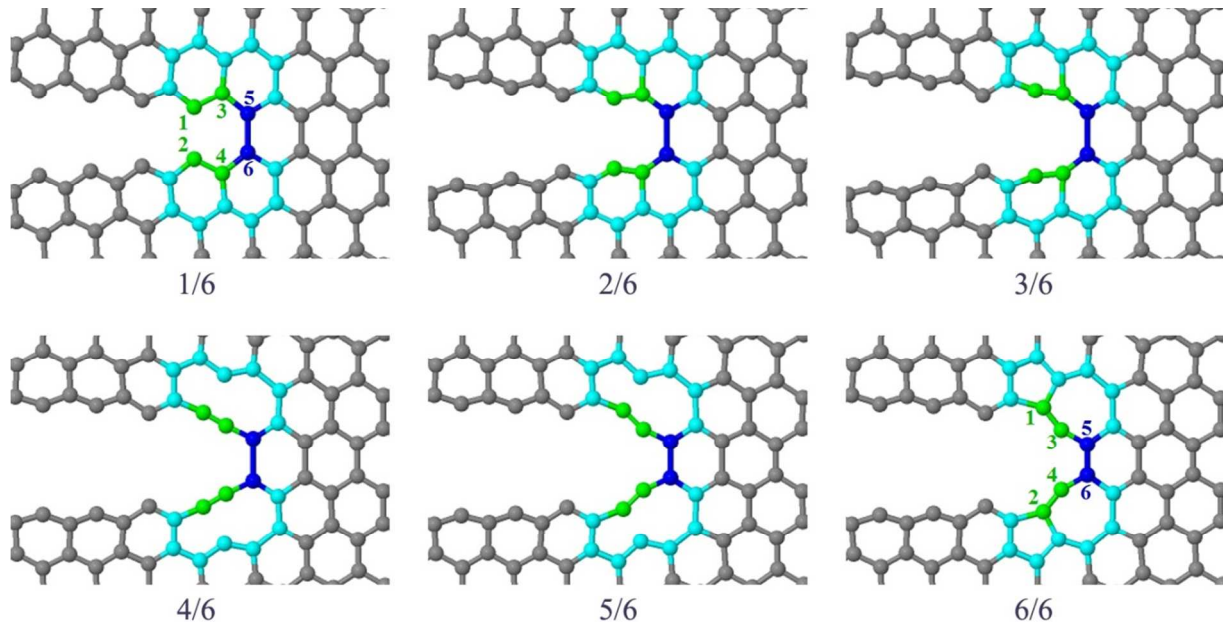


Figure 2. The mechanism of crack tip edge reconstruction during graphene fracture. As a result of the rotation of a pair of bonds (highlighted in green) near crack tip induced by the critical bond (highlighted in blue), the affected hexagonal cells (Step 1) gradually reconstruct into two pentagon-heptagon pairs (Steps 2-6).

Continuum Mechanics of Fracture. In continuum mechanics, we treat the monolayer graphene as an isotropic material due to its high level of symmetry.³² Besides being isotropic, graphene is also an elastic material with high brittleness and low plasticity, therefore Linear Elastic Fracture Mechanics (LEFM)³³ can be applied. LEFM states that whether a crack will heal or propagate depends solely on whether the local crack extension force, described by the stress intensity factor K_I - a concept introduced by Irwin's modification³⁴ of the Griffith theory - could overcome the inherent material resistance to cracking, described by the Fracture Toughness K_R regardless of the global stress condition of the material. The units of both quantities are $\text{eV}/\text{\AA}^{5/2}$. For material

under uniaxial load, one can obtain K_I from the equation: $K_I = Y\sigma\sqrt{\pi a}$, in which Y is a constant that depends on the crack opening mode and the geometry of the specimen, σ is the applied macroscopic stress, and a is the length of the crack.³³ For a constant σ , there is a crack length a_I that satisfies $K_I = K_R$. This a_I is exactly the critical crack length, as given by the Griffith theory.³³

Model of the Crack Tip. We create a model of the crack tip with the atoms placed according to the Griffith displacement field determined by the stress intensity factor K_I . According to the Griffith theory, the atom displacements in the x and y directions, designated by u_x and u_y , respectively, are given by:

$$\begin{cases} u_x = \frac{K_I}{2E} \sqrt{\frac{r}{2\pi}} (1 + \nu) [(2\kappa - 1) \cos\left(\frac{\theta}{2}\right) - \cos\left(\frac{3\theta}{2}\right)] \\ u_y = \frac{K_I}{2E} \sqrt{\frac{r}{2\pi}} (1 + \nu) [(2\kappa + 1) \sin\left(\frac{\theta}{2}\right) - \sin\left(\frac{3\theta}{2}\right)] \end{cases} \quad (8)$$

Here, K_I is the stress intensity factor, E is Young's modulus ($E = 1$ TPa for graphene), ν is Poisson's ratio ($\nu = 0.149$ for graphene), and $\kappa = (3 - \nu)/(1 + \nu)$ for in-plane stress.

Our model of cracking is a graphene sheet with 324 carbon atoms within the circular area near the crack tip. The atoms are placed according to the Griffith displacement field. Carbon atoms on the outer boundary are passivated with hydrogen atoms. The model is then geometrically optimized, with all the atoms within 2\AA from the outer boundary edge held fixed during the relaxation. In the optimized models (Figure 3b), the interior atoms assume the minimum energy configuration, reproducing the atomic conditions near the crack tip, while the boundary atoms are positioned according to the Griffith theory, providing a connection to the continuum macroscopic system outside of the model. If the

system is under a quasi-static load in which K_I is kept constant, our models serve as “snapshots” of the crack tip during the fracture process.

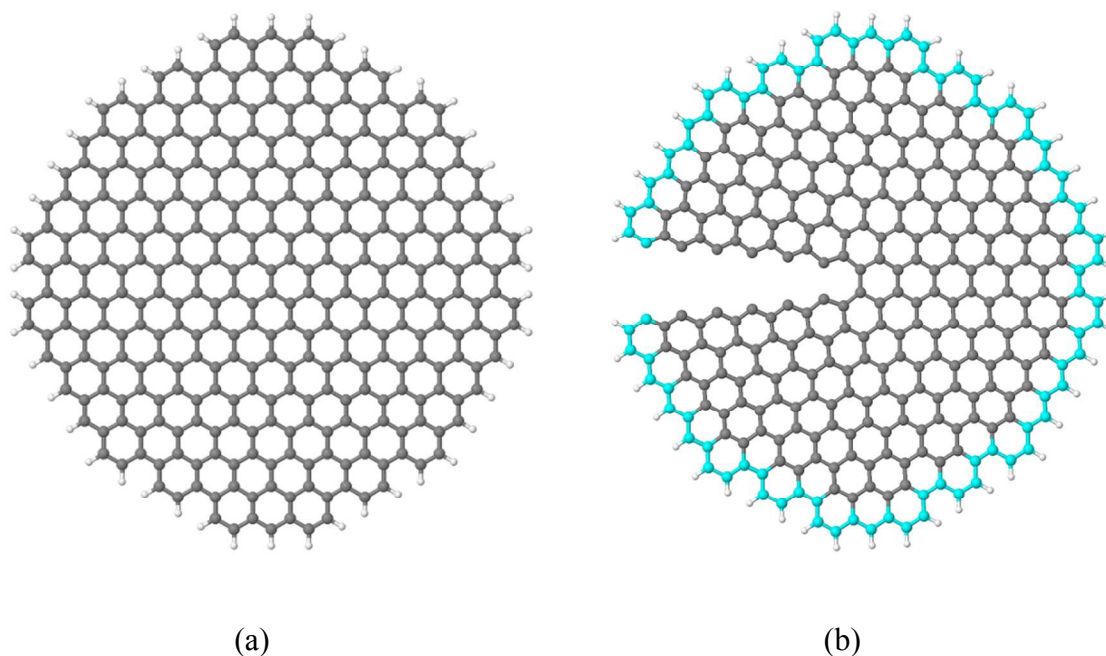


Figure 3. The atomistic crack tip model: (a) original configuration (b) with displacement field applied and geometry optimized. Boundary atoms (highlighted in cyan) are held fixed during the relaxation.

Three States of the Crack Tip. For a model of certain K_I , the atoms near the crack tip can assume several configurations describing the local state of the crack tip – bond intact (starting configuration), bond broken (after one crack propagation step), and reconstructed (after one crack propagation step), which are denoted as State A, B, and C, respectively. The positions of the boundary atoms in each state are the same as dictated by K_I . State A is the starting configuration of the system, in which the bond that is located exactly on the crack tip (designated as the “critical bond”) stays intact. State B is

the configuration in which the critical bond is broken; the atomic positions of State B can be regarded as that of State A translated by one lattice unit towards the direction of crack propagation. State C also originates from State A, but is a result of reconstruction (Figure 4) rather than bond breaking. During graphene fracture, a crack-tip model starting from the configuration of State A may choose either of the two processes: bond breaking (A to B), or reconstruction (A to C). The reconstruction process has been described in Figure 2, with State A as step 1 and State C as step 6.

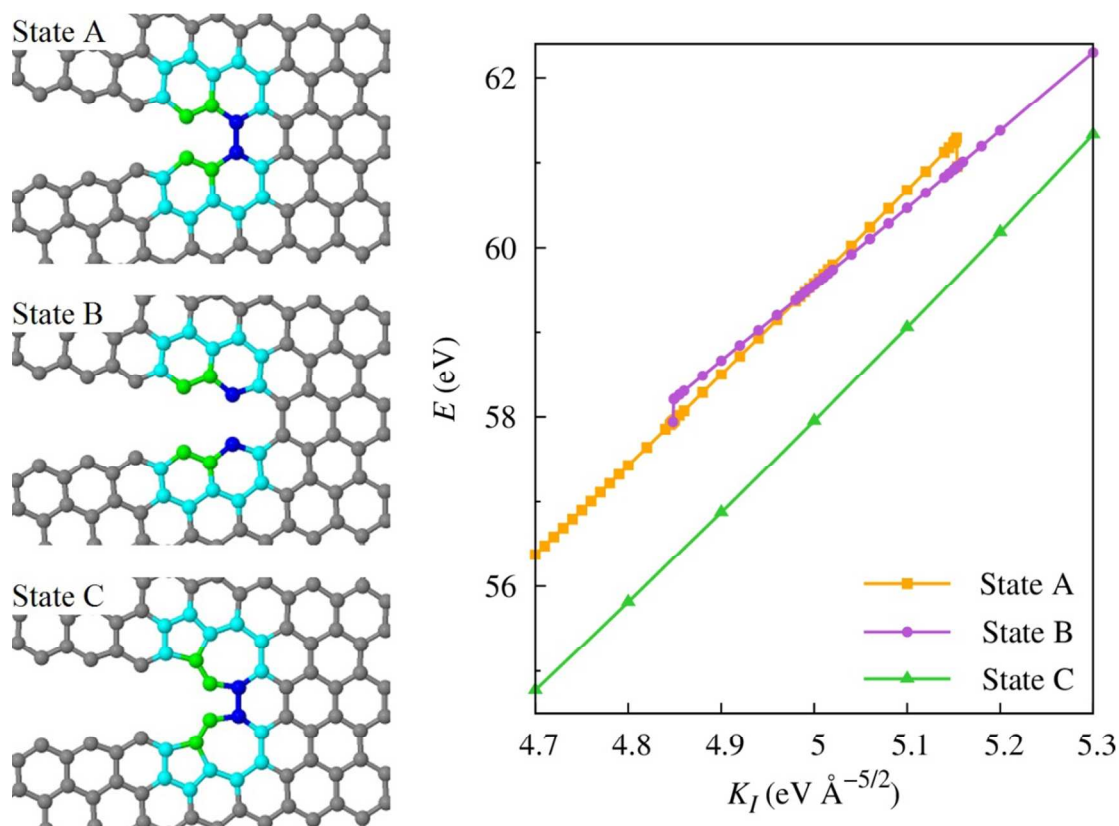


Figure 4. Comparison of the geometries (left) and energies (right) of States A, B and C under varying loads.

Mechanical Conditions for Reconstruction: “The Butterfly Zone.” We next find the range of the stress intensity factor K_I that allows the reconstruction process to occur at the crack tip. To obtain this range, we apply different loads to the models of State A and State B and let the models relax with the boundary atoms fixed. For the relaxed structures, the dependencies of their total energies E on the load K_I are shown in Figure 5a.

According to the relative values of the energy, the state of the system can be divided into three zones: Zone I, with the load range $K_I < 4.849 \text{ eV}/\text{\AA}^{5/2}$; Zone II, with the load range $4.849 \text{ eV}/\text{\AA}^{5/2} < K_I < 5.153 \text{ eV}/\text{\AA}^{5/2}$; and Zone III, with the load range $K_I > 5.153 \text{ eV}/\text{\AA}^{5/2}$.

We can see that in Zone I and Zone III, the energies of State A and State B overlap. In Zone I, models of State A are stable, while models of State B converge to State A. The reason is that in Zone I, K_I is lower than the required range of loads to create metastable states. Similarly in Zone III, models of State B are stable, while models of State B converge to State A. Macroscopically, models in Zone I and Zone III resemble the systems of crack healing and crack propagation in the Griffith theory.³¹ In these systems, reconstruction at the crack tip will not occur.

In Zone II, however, we observe a butterfly-like-pattern, suggesting the existence of metastable states. This phenomenon can be explained by the lattice trapping effect.^{33, 35} In continuum mechanics, the dependence of total free energy on the crack length is a smooth line with only one global maximum that corresponds to the critical crack length. At the atomistic scale, however, energy barriers for bond breaking need to be considered, resulting in minor corrugations of the total energy surface. In our models, the local energy corrugation is not negligible compared to the system total energy, and the lattice

trapping effect can be observed. States A and B can both exist under the same load in Zone II, because there is an activation energy barrier between the two states, and the transition from each state to the other requires overcoming this barrier.

In the “butterfly zone” (Zone II) the two separate lines split at $K_I^- = 4.849 \text{ eV/\AA}^{5/2}$, cross each other at the Griffith load $K_I^C = 4.990 \text{ eV/\AA}^{5/2}$, and merge at $K_I^+ = 5.153 \text{ eV/\AA}^{5/2}$ (Figure 5). For $K_I = K_I^C = 4.990 \text{ eV/\AA}^{5/2}$ ((3) in Figure 5), the two local states A and B are isoenergetic³². To the left hand side of K_I^C , ($K_I^- < K_I < K_I^0$), the energy surface tilts towards State A, and the barrier is lower for bond healing than for bond breaking ((2) in Figure 5), until at $K_I = K_I^- = 4.849 \text{ eV/\AA}^{5/2}$ ((1) in Figure 5), the barrier for bond healing vanishes, and both State A and State B collapse into State A, resulting in an ‘uphill’ transition. Symmetrically, to the right hand side of K_I^C ($K_I^0 < K_I < K_I^+$), the energy surface tilts towards State B, and barrier will be lower for bond breaking than for bond healing ((4) in Figure 5), until at $K_I = K_I^+ = 5.153 \text{ eV/\AA}^{5/2}$, ((5) in Figure 5), the barrier for bond breaking vanishes, and both State A and State B collapse into State B, resulting in a ‘downhill’ transition.

From the discussion above we can see that Zone II is the required range of load K_I for reconstruction at crack tip. With this mechanical condition established, we proceed to analyze thermodynamic and kinetic conditions for crack tip reconstruction during fracture.

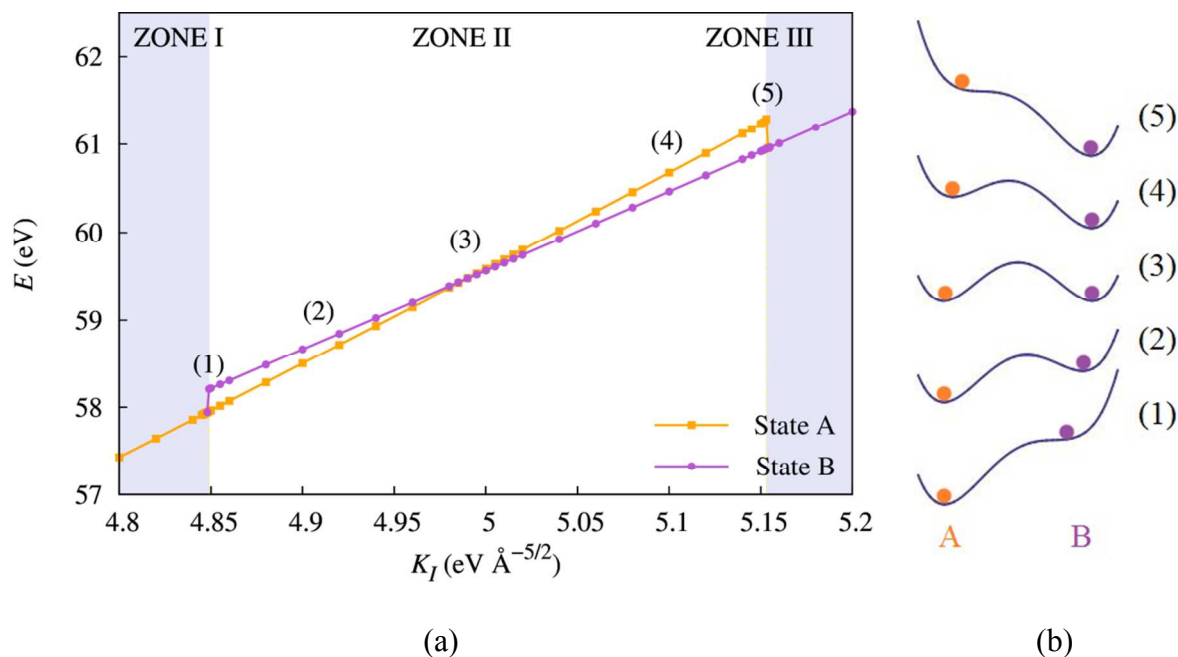


Figure 5. The energetics of lattice trapping effect. (a) The three zones and the butterfly pattern in Zone II (b) Total energy dependence of the model going from State A to State B, under different loads. (Inspiration of plot from SL Zhang *et al.*³²)

Energetics of Reconstruction. It is evident that reconstruction at the crack tip is thermodynamically favorable, as can be seen from the energetics of pristine vs. reconstructed structures under varying load. In Figure 4, the energy comparison of States A, B, and C are shown. One can see that $E_A > E_C$ and $E_B > E_C$ for the entire Zone II, with the energy difference of $\Delta_E \sim 2.37$ eV (at $K_I = K_I^c$). This large energy difference suggests that under these mechanical conditions reconstruction at the crack tip is always thermodynamically favorable.

For the kinetic part of the analysis, we need to determine the activation energy barrier for the reconstruction process of paired bond rotation. The barrier is found by performing a Nudged Elastic Band (NEB) calculation between States A and C, under the metastable

load $K_I = K_I^{rec} = 4.990 \text{ eV}/\text{\AA}^{5/2}$. The transitional process obtained by NEB is shown in Figure 2. The barrier computed for paired bond rotation is $E_{rec} = 0.98 \text{ eV}$, while for single reconstruction on free-standing edge is $E_{rec}^{single} = 0.93 \text{ eV}$. The fact $E_{rec} < 2 \times E_{rec}^{single}$ suggests that the fracture process of graphene significantly enhances edge reconstruction by coupling stress with bond rotations.

The reaction rates of reconstruction at crack tip can be obtained using the Arrhenius equation:

$$k_{rec} = A e^{-E_{rec}/k_B T} = \begin{cases} 2 \times 10^{-4} \text{ s}^{-1} (300 \text{ K}) \\ 7 \times 10^2 \text{ s}^{-1} (500 \text{ K}) \\ 6 \times 10^7 \text{ s}^{-1} (1000 \text{ K}) \end{cases} \quad (9)$$

Here, $A = 5 \times 10^{12} \text{ s}^{-1}$ is the attempt frequency, taken from the G-mode vibration of graphene at 1580 cm^{-1} , and k_B is the Boltzmann Constant. The reaction rate results show that at room temperature, reconstruction has a low chance of occurring at the crack tip (although still possible); at elevated temperatures, the chance increases dramatically.

The activation barrier for direct bond breaking at crack tip (from State A to State B) is $E_{break} = 0.10 \text{ eV}$, which is much lower than that of paired bond rotation, suggesting that at pristine crack tips of graphene (the ones with no previously formed pentagon-heptagon pairs), simple bond breaking is still the dominating process (Figure 6a).

At the crack tip with fully reconstructed edges, however, a subsequent reconstruction is a very favorable process. We calculated the energetics of the models corresponding to states A, B and C, the only difference being that there are pre-existing pentagon-heptagon pairs near the crack tip. Comparison between first-step and subsequent reconstructed structures is shown in Figure 6. The energy reward of reconstruction rises from the $\Delta_E \sim 2.37 \text{ eV}$ of crack tip with pristine edges to $\Delta_E \sim 2.53 \text{ eV}$, while the activation

energy barrier decreases from 0.98 eV to 0.63 eV. We point out that, for this pre-reconstructed crack tip, the activation energy barrier for simple bond breaking rises from 0.10 eV to 0.73 eV, possibly due to the release of elastic tension by pentagon-heptagon pairs. These results indicate that once successfully initiated, subsequent reconstruction processes at the crack tip become both thermodynamically and kinetically more favorable than bond breaking, therefore, it is highly possible to obtain ZZ57 edges during graphene fracture (Figure 6b).

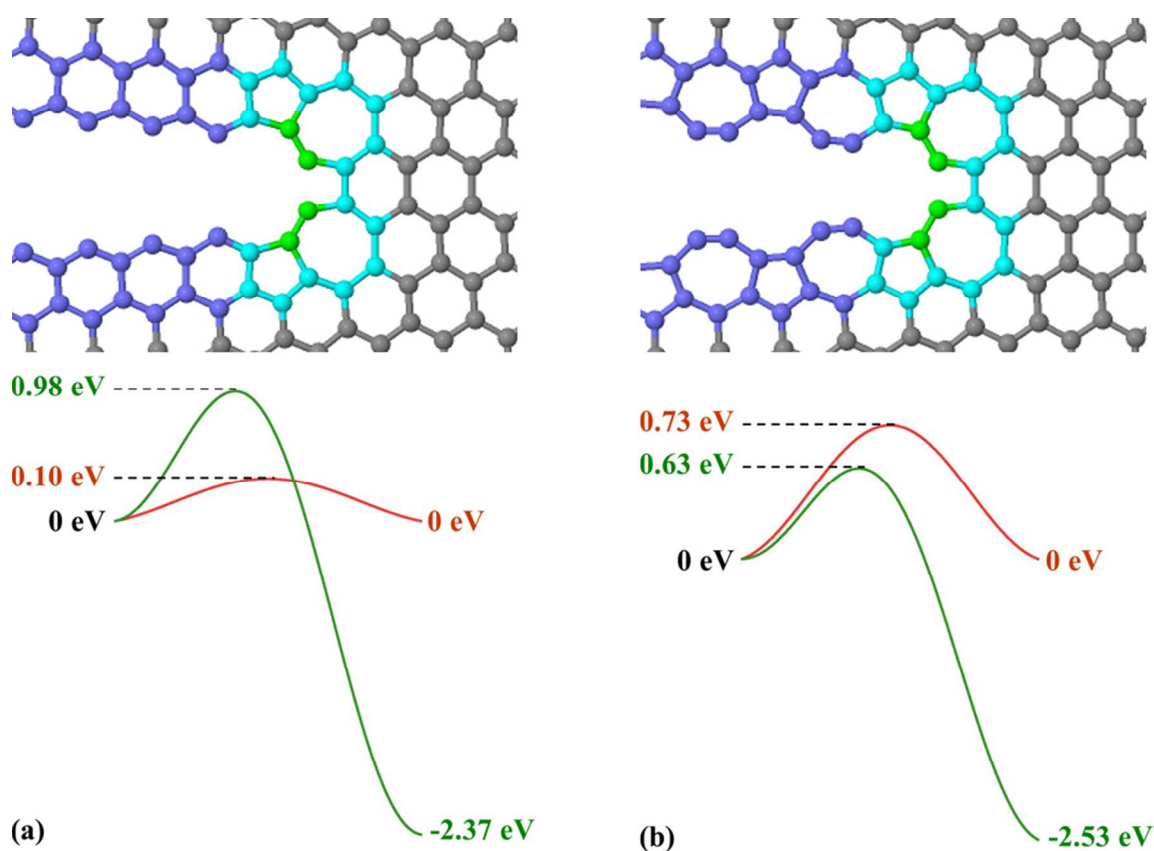


Figure 6. Structural and energetic comparison between first-step (a) and subsequent (b) crack tip reconstructions. The red lines are for bond breaking and the green lines are for reconstruction. Both energy reward and transition barrier show that once reconstruction is initiated, its propagation becomes much easier, suggesting the possibility of obtaining

ZZ57 edges during fracture.

Will the Pentagon-Heptagon Pairs Last? Before drawing the final conclusion, however, one needs to make sure that the newly-formed pentagon-heptagon pairs are stable. According to Terdalkar *et al.*³⁰ further bond rotations may occur on the pentagon-heptagon pairs, leading to the separation of pentagons and heptagons by hexagons. This process, if possible, would be detrimental for obtaining clean reconstructed edges. Here we show its impossibility by comparing it with direct bond breaking right after the reconstruction.

In Figure 7, State C shows the state of the crack tip right after the first reconstruction (identical to the aforementioned State C), State D represents the crack tip with the two connecting bonds broken (from the simulation results we know that the two bonds are actually coupled, i.e. they stay intact or broken together), and State E shows what the crack tip would be if the two bonds highlighted in green rotated. We calculate the energies of the models in the three states and compare them as shown in Figure 7.

From Figure 7 we can see that, around the metastable load for State C: $K_I \sim 5.0 \text{ eV}/\text{\AA}^{5/2}$, the energy cost for the pentagon and heptagon to separate from each other is as high as $\Delta E = E_E - E_C \sim 3.66 \text{ eV}$ (while that of the bond breaking is $\Delta E = E_D - E_C \sim 0 \text{ eV}$). NEB results show that the activation barrier is 5.95 eV for separation, and 0.98 eV for the bond breaking. As we can see, both thermodynamic and kinetic analysis strongly disfavor the separation of pentagons and heptagons, suggesting this process is unlikely to hinder the formation of clean ZZ57 edges during fracture.

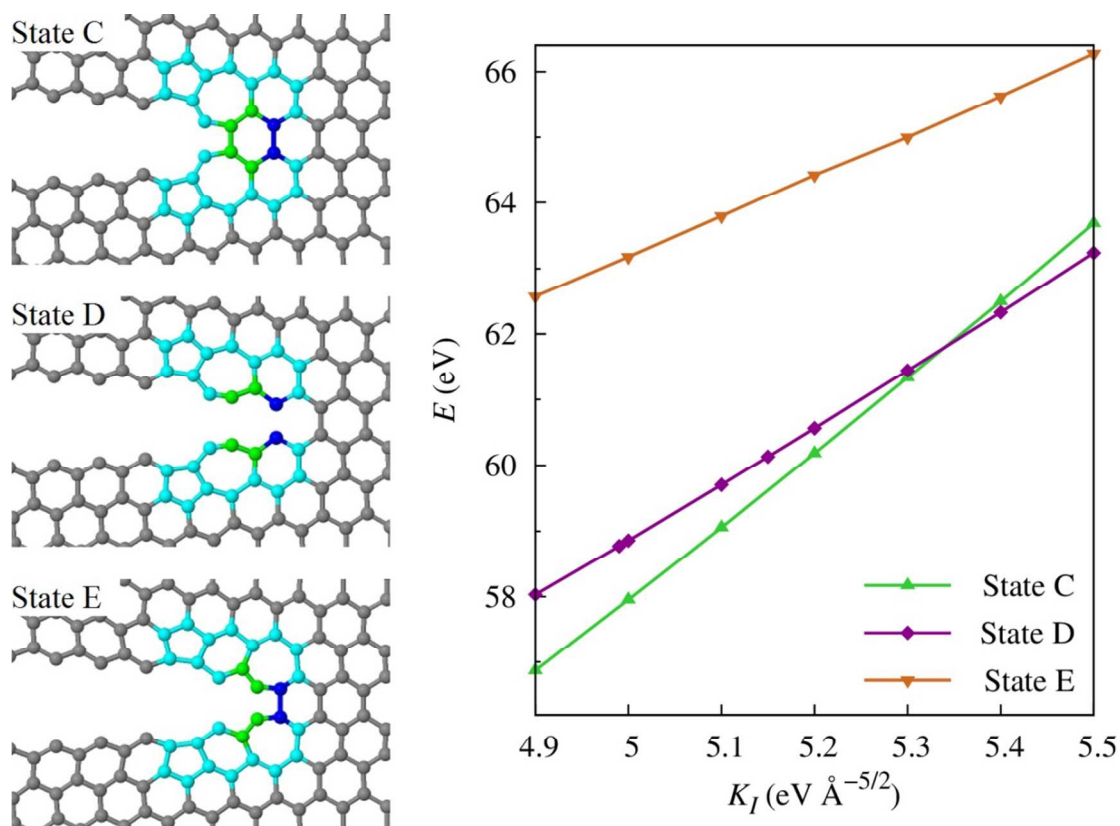


Figure 7. Comparison of the geometries (left) and energies (right) of States C, D and E under varying loads.

Conclusions

To summarize, we have studied the process of edge reconstruction at the crack tip during the mechanical fracture of graphene, in which pentagon-heptagon pairs, the component of ZZ57 edge – the most stable edge of any configuration or chirality based on our analytical formula – can be obtained. By analyzing its mechanism and conditions, we confirm that pentagon-heptagon pairs can form at the crack tip, and that it is possible to obtain ZZ57 edges by mechanically fracturing graphene sheet, since the pentagon-heptagon pairs are stable, allowing subsequent reconstructions to occur with much more

favorable energetics. We provide a simple guideline for forming different types of edges during graphene fracture – namely, apply low load and high temperature to favor the formation of ZZ57 edges, and high load and low temperature to favor the formation of ZZ edges.

Methods

For the energetics of free-standing graphene edges, we used Vienna Ab-initio Simulation Package (VASP),^{36, 37} with projector augmented wave (PAW) pseudopotentials,^{38, 39} and Perdew–Burke–Ernzerhof (PBE)⁴⁰ generalized gradient approximation (GGA) for the exchange-correlation functional. First-principle calculations are well suited for evaluating the complicated energetics of dangling bonds on ZZ edges and triple bonds on ZZ57 edges.

For the simulation of fracture process, we employed Density Functional with Tight Binding (DFTB)⁴¹. The DFTB method is far more accurate and transferable than classical potentials since it is parameter-free on second order, and thus avoids the errors caused by the empirical parameters of traditional bond-order potentials. In particular, classical bond order potentials give unphysical bond breaking behavior due to the well-known spiking of the force near the energy cutoff distance. DFTB is also expected to give more accurate description of graphene elastic properties and edge formation energies.

For the large system that was used here for modeling graphene crack tip fracture, DFTB provided a reasonable tradeoff between computational speed and accuracy. To further test the accuracy of the DFTB method, we compared the formation energies of free-standing graphene edges yielded by DFTB and the density functional theory (DFT),

as computed with VASP. The results show that DFTB can achieve a high degree of accuracy even in comparison with a more accurate DFT.

Atomistic visualizations of the graphene fracture were performed using Jmol.⁴²

Acknowledgements

Computations were performed on the DAVinCI and Sugar clusters sponsored by funds from NSF grant OCI-0959097.

References

1. Geim, A. K.; Novoselov, K. S. *Nat Mater* **2007**, 6, (3), 183-191.
2. Lee, C.; Wei, X. D.; Kysar, J. W.; Hone, J. *Science* **2008**, 321, (5887), 385-388.
3. Castro Neto, A. H.; Guinea, F.; Peres, N. M. R.; Novoselov, K. S.; Geim, A. K. *Rev Mod Phys* **2009**, 81, (1), 109-162.
4. Meyer, J. C.; Geim, A. K.; Katsnelson, M. I.; Novoselov, K. S.; Booth, T. J.; Roth, S. *Nature* **2007**, 446, (7131), 60-63.
5. Yan, Q. M.; Huang, B.; Yu, J.; Zheng, F. W.; Zang, J.; Wu, J.; Gu, B. L.; Liu, F.; Duan, W. H. *Nano Lett* **2007**, 7, (6), 1469-1473.
6. Pumera, M. *Chem Rec* **2009**, 9, (4), 211-223.
7. Hu, Y. H.; Wang, H.; Hu, B. *Chemsuschem* **2010**, 3, (7), 782-796.
8. Son, Y. W.; Cohen, M. L.; Louie, S. G. *Nature* **2006**, 444, (7117), 347-349.
9. Wakabayashi, K.; Fujita, M.; Ajiki, H.; Sigrist, M. *Phys Rev B* **1999**, 59, (12), 8271-8282.
10. Fujita, M.; Wakabayashi, K.; Nakada, K.; Kusakabe, K. *J Phys Soc Jpn* **1996**, 65, (7), 1920-1923.
11. Nakada, K.; Fujita, M.; Dresselhaus, G.; Dresselhaus, M. S. *Phys Rev B* **1996**, 54, (24), 17954-17961.
12. Bets, K. V.; Yakobson, B. I. *Nano Res* **2009**, 2, (2), 161-166.
13. Ritter, K. A.; Lyding, J. W. *Nat Mater* **2009**, 8, (3), 235-242.
14. Liu, Y.; Dobrinsky, A.; Yakobson, B. I. *Phys Rev Lett* **2010**, 105, (23), 235502.
15. Koskinen, P.; Malola, S.; Hakkinen, H. *Phys Rev Lett* **2008**, 101, (11), 115502.
16. Koskinen, P.; Malola, S.; Hakkinen, H. *Phys Rev B* **2009**, 80, (7), 073401.

17. Girit, C. O.; Meyer, J. C.; Erni, R.; Rossell, M. D.; Kisielowski, C.; Yang, L.; Park, C. H.; Crommie, M. F.; Cohen, M. L.; Louie, S. G.; Zettl, A. *Science* **2009**, 323, (5922), 1705-1708.
18. Kim, K.; Coh, S.; Kisielowski, C.; Crommie, M. F.; Louie, S. G.; Cohen, M. L.; Zettl, A. *Nat Commun* **2013**, 4, 2723.
19. Rodrigues, J. N. B.; Goncalves, P. A. D.; Rodrigues, N. F. G.; Ribeiro, R. M.; dos Santos, J. M. B. L.; Peres, N. M. R. *Phys Rev B* **2011**, 84, (15), 155435.
20. Dubois, S. M. M.; Lopez-Bezanilla, A.; Cresti, A.; Triozon, F.; Biel, B.; Charlier, J. C.; Roche, S. *Acs Nano* **2010**, 4, (4), 1971-1976.
21. Cheng, Y. C.; Wang, H. T.; Zhu, Z. Y.; Zhu, Y. H.; Han, Y.; Zhang, X. X.; Schwingenschlogl, U. *Phys Rev B* **2012**, 85, (7), 073406.
22. Song, L. L.; Zheng, X. H.; Wang, R. L.; Zeng, Z. *J Phys Chem C* **2010**, 114, (28), 12145-12150.
23. Gao, J. F.; Zhao, J. J.; Ding, F. *J Am Chem Soc* **2012**, 134, (14), 6204-6209.
24. Kroes, J. M. H.; Akhukov, M. A.; Los, J. H.; Pineau, N.; Fasolino, A. *Phys Rev B* **2011**, 83, (16), 165411.
25. Soldano, C.; Mahmood, A.; Dujardin, E. *Carbon* **2010**, 48, (8), 2127-2150.
26. Kim, K.; Artyukhov, V. I.; Regan, W.; Liu, Y. Y.; Crommie, M. F.; Yakobson, B. I.; Zettl, A. *Nano Lett* **2012**, 12, (1), 293-297.
27. Huang, X.; Yang, H.; van Duin, A. C. T.; Hsia, K. J.; Zhang, S. L. *Phys Rev B* **2012**, 85, (19), 195453.
28. Huang, S.; Zhang, S. L.; Belytschko, T.; Terdalkar, S. S.; Zhu, T. *J Mech Phys Solids* **2009**, 57, (5), 840-850.
29. Zhang, B.; Mei, L.; Xiao, H. F. *Appl Phys Lett* **2012**, 101, (12), 121915
30. Terdalkar, S. S.; Huang, S.; Yuan, H. Y.; Rencis, J. J.; Zhu, T.; Zhang, S. L. *Chem Phys Lett* **2010**, 494, (4-6), 218-222.
31. Griffith, A. A. *Philosophical Transactions of the Royal Society of London, Series A* **1921**, 221, 163-198.
32. Zhang, S. L.; Zhu, T.; Belytschko, T. *Phys Rev B* **2007**, 76, (9), 094114.
33. Meyers, M. A.; Chawla, K. K., *Mechanical Behavior of Materials*. Cambridge University Press: 2008.
34. Irwin, G. R. *Journal of Applied Mechanics* **1957**, 24, 361-364.

35. Dumitrica, T.; Belytschko, T.; Yakobson, B. I. *J Chem Phys* **2003**, 118, (21), 9485-9488.
36. Kresse, G.; Furthmuller, J. *Comp Mater Sci* **1996**, 6, (1), 15-50.
37. Kresse, G.; Furthmuller, J. *Phys Rev B* **1996**, 54, (16), 11169-11186.
38. Blochl, P. E. *Phys Rev B* **1994**, 50, (24), 17953-17979.
39. Kresse, G.; Joubert, D. *Phys Rev B* **1999**, 59, (3), 1758-1775.
40. Perdew, J. P.; Burke, K.; Ernzerhof, M. *Phys Rev Lett* **1996**, 77, (18), 3865-3868.
41. Elstner, M.; Porezag, D.; Jungnickel, G.; Elsner, J.; Haugk, M.; Frauenheim, T.; Suhai, S.; Seifert, G. *Phys Rev B* **1998**, 58, (11), 7260-7268.
42. Jmol: an open-source Java viewer for chemical structures in 3D. <http://www.jmol.org/>